17 May 2002

ELSEVIER

Chemical Physics Letters 357 (2002) 327–335

CHEMICAL PHYSICS LETTERS

www.elsevier.com/locate/cplett

Multiple quantum coherences in liquid state NMR and nonlinear optics: collective vs local origin

Shaul Mukamel *, Andreas Tortschanoff

Department of Chemistry and Rochester Theory Centre for Optical Science and Engineering, University of Rochester, P.O. RC Box 270216, Rochester, NY 14627-0216, USA

Received 17 December 2001; in final form 5 February 2002

Abstract

Recently observed high harmonic multi-particle echo resonances (multiple quantum coherence) in NMR have been interpreted using either direct coupling or local-field mechanisms. We show that a unified picture for both mechanisms may be obtained by calculating the signals perturbatively in the incoming pulses in terms of response functions using a many-body approach originally developed for nonlinear optics. Specific signatures which can distinguish between the two are identified, and new double quantum resonances of both types are predicted in four-wave mixing in the direction $\mathbf{k}_1 + \mathbf{k}_2 - \mathbf{k}_3$.

Even though the calculation of NMR signals is a complex many-body problem involving the dynamics of a macroscopic number of coupled spins, most experiments may be readily interpreted by solving the Bloch equations for a single spin. Surprising effects which show up in liquid NMR when large nuclear magnetizations are present were reported over the past 20 years [1–3]. These effects which include frequency shifts, multiple spin echoes, and additional peaks in two-dimensional spectra cannot be accounted for using the standard NMR theory. The recent study of high harmonic resonances in multiple pulse NMR which are signatures of intermolecular multiple quantum coherences (MQCs) [4,5] had triggered an extensive theoretical and experimental activity [6–8] and resulted in exciting novel applications to spectroscopy and MRI [9]. The simplest way to account for these resonances is by replacing the average magnetic field by the local-field which includes the macroscopic magnetization [1–3,6–8]. This classical local-field (LF) approximation retains the simplicity of the standard theory since it considers a single spin driven by a local-field. The LFMQC implies long-range coherence between spins which are microns apart. An alternative picture attributes these resonances to direct couplings between spins. This coupling-induced coherence CIMQC is related to correlations among spins. Both the classical, mean-field approach and the coupled-spin approach give quantitative predictions of signal intensity. The two mechanisms usually lead to identical signals (ignoring

* Corresponding author. Fax: +1-716-473-6889.
E-mail address: mukamel@chem.rochester.edu (S. Mukamel).

0009-2614/02/$ - see front matter
PII: S0009-2614(02)00408-6

relaxation and macroscopic molecular diffusion) [4,6,7,10,11].

In this Letter we show how both mechanisms may be analyzed and clearly distinguished using a unified, weak field, many-body, theoretical approach originally developed for nonlinear optics [12–16]. Our analysis provides an intuitive physical interpretation and establishes a connection between these NMR resonances and several many-body effects in nonlinear optics which have been extensively studied both experimentally and theoretically.

The connection between the optical and NMR experiments is not obvious at first glance due to many important differences [17,18]. First, in optical measurements the sample is typically larger than the optical wavelength. Coherent signals are thus generated only in specific directions which satisfy *phase matching*. In four-wave mixing carried out with three beams with wavevectors $\mathbf{k}_1$, $\mathbf{k}_2$, $\mathbf{k}_3$ the signal is only generated in the directions $\pm\mathbf{k}_1 \pm \mathbf{k}_2 \pm \mathbf{k}_3$. In contrast, in NMR the sample size is typically much smaller than the radio frequency wavelength, the $\mathbf{k}_j$ factors are not important, and the signal is generated in all directions. Nevertheless, the phase information contained in the optical wavevectors may be retrieved in NMR by scanning the phases of the various fields (phase cycling). Signatures of both mechanisms are more easily sorted out in nonlinear optics where phase matching at different wavevectors allows a clear identification of various contributions. The same separation in NMR requires phase cycling of the various pulses. Second, in NMR the temperature is typically high compared with transition frequency (which considerably simplifies the calculations since the equilibrium density matrix may be calculated classically) whereas in optics the opposite limit holds. Third, field gradients are effectively used in NMR but not in the optical regime to control the frequency and provide spatial resolution. Fourth, NMR experiments are usually conducted using strong saturating fields which maximize the signals and create specific combinations of *Liouville space pathways*. Nonlinear optical spectroscopy, in contrast, usually uses weak fields and is recast in terms of response functions obtained by a perturbative expansion in the incoming pulses. We argue that despite these differences between NMR and optical experiments, the underlying physics involving coherence transfer pathways is identical, allowing to draw analogies between the two and obtain a common qualitative picture of the origin of these resonances.

The weak field expansion carried out in this Letter simplifies the analysis considerably, allows a systematic treatment of the mechanism for the formation of these new resonances, and provides a very clear physical insight, which removes many of the mysteries. Such expansions should be very useful in the analysis of NMR signals since the origin of many NMR signals and resonances may be readily traced back to weak fields [12]. Weak field analysis of the NMR high harmonic resonances in terms of response functions should reveal the origin and key characteristics of the new resonances, making it possible to pinpoint their microscopic or macroscopic origin. We show that the interplay of both mechanisms should provide interesting new probes which distinguish between the short- and long-range origin of MQC. New effects, e.g high harmonic optical echoes in four-wave mixing at specific wavevectors can be predicted drawing upon the optical/NMR analogy. NMR is the elder brother of optical spectroscopy and many important effects first discovered in NMR have been found in the optical regime 20–30 years later. In this case, NMR may benefit from the more advanced treatment of many-body effects developed for optical spectroscopy.

The local-field approximation is based on the observation that in condensed phases each molecule is driven by an external local-field E_{l} which is different from the average (Maxwell) field E. In the long wavelength limit the two fields are related by the Lorentz formula [19,20] $E_{\mathrm{l}}(t) = E(t) + (4\pi/3)P(t)$, where $P(t)$ is the polarization per unit volume. The polarization of a single molecule (or a group of coupled molecules) can be expanded in terms of its response functions (polarizabilities) $\alpha, \beta, \gamma, \ldots$ to various orders in E_{l}. Both P and E_{l} can be expanded perturbatively in powers of E.

The nonlinear polarization $P^{\mathrm{NL}} = P^{(2)} + P^{(3)} + \cdots$ per unit volume of a macroscopic

sample made out of identical such molecules is given by [12]

$$P^{\mathrm{NL}}(\mathbf{r},t)=\rho_0\int_{-\infty}^{t}\mathrm{d}\tau_3\int_{-\infty}^{\tau_3}\mathrm{d}\tau_2\int_{-\infty}^{\tau_2}\mathrm{d}\tau_1 S(t-\tau_3)\times\beta(\tau_3,\tau_2,\tau_1)E_{\mathrm{l}}(\mathbf{r},\tau_2)E_{\mathrm{l}}(\mathbf{r},\tau_1)+\cdots, \quad (1)$$

where

$$E_{\mathrm{l}}(\mathbf{r},\tau)=\int_{-\infty}^{\tau}\mathrm{d}\tau' S(\tau-\tau')E(\mathbf{r},\tau')+\frac{4\pi}{3}\int_{-\infty}^{\tau}\mathrm{d}\tau' S(\tau-\tau')P^{\mathrm{NL}}(\mathbf{r},\tau') \quad (2)$$

$S(t)$ defined after Eq. (3) represents the contribution of the linear polarization $P^{(1)}$ to the local field and ρ_0 is the number density of spins.

Upon the substitution of Eq. (2) in Eq. (1) we obtain an integral equation for P^{NL} whose iterative solution results in the desired expansion of P^{NL} in powers of E which may be directly used to compute optical signals. The first term in the RHS of Eq. (2) is responsible for *local-field* effects whereas the second term generates *cascading* contributions to the nonlinear response. Cascading effects are very interesting, may contribute to these new resonances and deserve a separate study. As a result of cascading, E_{l} may contain multiples of molecular frequencies ω_0. For example, $E_{\mathrm{l}}^{(3)}$ will contain terms generated locally by harmonic generation, oscillating at $3\omega_0$. Successively higher frequencies are generated at higher orders. Hereafter we neglect cascading, i.e. the second term in Eq. (2) since the local-field effects are enough to generate the new resonances. We then obtain for the third-order polarization which generates the four wave mixing signal [12]

$$P^{(3)}(\mathbf{r},t)=\rho_0\int_{-\infty}^{t}\mathrm{d}\tau_4\int_{-\infty}^{t}\mathrm{d}\tau_3\int_{-\infty}^{\tau_3}\mathrm{d}\tau_2\times\int_{-\infty}^{\tau_2}\mathrm{d}\tau_1 S(t-\tau_4)\gamma(\tau_4,\tau_3,\tau_2,\tau_1)\times E_{\mathrm{l}}(\mathbf{r},\tau_1)E_{\mathrm{l}}(\mathbf{r},\tau_2)E_{\mathrm{l}}(\mathbf{r},\tau_3), \quad (3)$$

with the Clausius–Mossotti relation

$$E_{\mathrm{l}}(\mathbf{r},\tau)=\int_{-\infty}^{\tau}\mathrm{d}\tau' S(t-\tau')E(\mathbf{r},\tau'),$$

where $S(\omega)=[1-(4\pi/3)\rho_0\alpha(\omega)]^{-1}$ is the Fourier transform of $S(t)$ and γ is the cubic polarizability.

At the local-field level the complex many-body problem thus reduces to a single-body calculation of polarizabilities. Local-field-induced resonances come when solving Maxwell's equations for the *transverse* Maxwell field and are contained in $S(\tau)$. They exist even in the absence of direct intermolecular couplings. Formally all additional LF-resonances or observed features carry no new information since they only use the polarizabilities of noninteracting molecules as an input. However, in NMR, using field gradients it is possible to control the local frequencies and gain spatial information which found important applications to, e.g. MRI [9]. On the other hand collective resonances can also arise from direct Coloumb intermolecular interactions in the molecular Hamiltonian which represent the *longitudinal* electric field and enter Eq. (3) via γ. CIMQC resonances carry additional microscopic information and can be clearly separated from local-field contributions to the high harmonics using this approach. The transverse and longitudinal fields are clearly separable when using the Coulomb gauge [21].

Since both mechanisms enter the signal in a different way (i.e. via S or γ), we expect some distinct differences between both types of resonances. For example the time evolution and phase of the signal should be different and clearly distinguishable.

Let us consider a impulsive four-wave mixing process carried out with three well-separated short pulses with wavevectors $\mathbf{k}_1$, $\mathbf{k}_2$, $\mathbf{k}_3$ whose spectral bandwidths cover the entire manifold of states. We expand the field in modes $E(\mathbf{r},t)=\sum_j E_j(t)\exp(-\mathrm{i}\omega_j t+\mathrm{i}\mathbf{k}_j\mathbf{r})+c.c.$ $P^{\mathrm{NL}}(\mathbf{r},t)$ and $E_{\mathrm{l}}(\mathbf{r},t)$ can be expanded similarly. Pulse 1 comes first, then 2, and finally 3. We shall look for the origin of double quantum $\omega_1+\omega_2$ resonances after the application of two pulses for uncoupled two-level molecules or spins and neglect local-field effects by setting $S(\tau-\tau')=\delta(\tau-\tau')$ and replacing E_{l} by E. γ is now the third-order polarizability of an isolated spin. After interactions with two pulses the system must be in a population grating oscillating at $\omega_1-\omega_2$ and no two-quantum $\omega_1+\omega_2$ resonances can be generated. This is why the standard NMR theory misses these resonances.

One important consequence of this is that the four-wave mixing signal generated in the direction $\mathbf{k}_{\mathrm{RPE}} = \mathbf{k}_1 + \mathbf{k}_2 - \mathbf{k}_3$ known as the reverse photon echo (RPE) vanishes identically for this model [22–24]. The entire RPE signal must therefore be induced by many-body effects, making this technique an ideal probe for these effects. Hereafter we shall focus on this technique.

Both local-field and intermolecular couplings incorporated in Eq. (3) can give rise to $\omega_1 + \omega_2$ resonances, the former entering through $S(\tau)$ whereas the latter via γ. To see how the distinction between CIMQC and LFMQC can be unambigiously made, we consider first the effects of intermolecular couplings. We assume short (impulsive) pulses and neglect local-fields, setting $S(\tau - \tau') = \delta(\tau - \tau')$. Since the molecules are coupled their eigenstates form distinct manifolds of states (single-exciton $|e\rangle$, two-exciton $|f\rangle$, etc. (inset of Fig. 2b)). Their couplings are short range and correspond, e.g. to two spins on the same molecule. Now the $\mathbf{k}_{\mathrm{RPE}}$ signal does exist and shows $\omega_1 + \omega_2$ resonances. The corresponding double-sided Feynman diagrams are shown in Fig. 1a. Each diagram represents a *Liouville Space Pathway* showing the time evolution of the density matrix for a specific sequence of couplings with the pulse. Time goes from bottom to top. The left (right) line represents the ket (bra) of the density matrix. Arrow pointing to the right (left) represents a $+\mathbf{k}(-\mathbf{k})$ contribution. In the left diagram the density matrix changes from $|g\rangle\langle g|$ to $|f\rangle\langle g|$ (during the interval t_{23}) and then to $|e\rangle\langle g|$ where the signal $\mathbf{k}_{\mathrm{RPE}}$ is generated. In the right diagram we have $|g\rangle\langle g|$ to $|f\rangle\langle g|$ and to $|f\rangle\langle e|$. [See Chapter 6 of [9] for the detailed rules for these diagrams.]

Turning next to uncoupled molecules with local-field effects included, we have calculated E_1 to lowest order in molecular density. We assume a short pulse $E(t) \propto \delta(t - T)$ and calculate E_1 to lowest order in molecular density, resulting in

$$E_1^{(1)}(t) = E(t) + \frac{4\pi}{3}\rho_0\alpha(t - T), \tag{4}$$

where $\alpha(\tau) \propto \sin(\omega_0\tau)\exp(-\Gamma\tau)$. In this case the local-field destroys the time ordering of the incident fields, and allows the generation of the $\mathbf{k}_{\mathrm{RPE}}$ signal, as shown by the Feynman diagrams of Fig. 1b, c. The $\mathbf{k}_2$ Maxwell field interacts with molecule A creating a local-field. The initial pulse $E(t)$ is very short (impulsive). If the dephasing rate Γ is not too large, the local-field is much longer than the Maxwell field. Molecule B can then interact with $\mathbf{k}_1$, then with $\mathbf{k}_3$ and finally with the $\mathbf{k}_2$ component of the local-field generated by molecule A. This time-ordering is not possible without local-field corrections since the 1, 2, 3, order is then strictly enforced. During the interval between pulses 2 and 3, there are two molecules in a co-

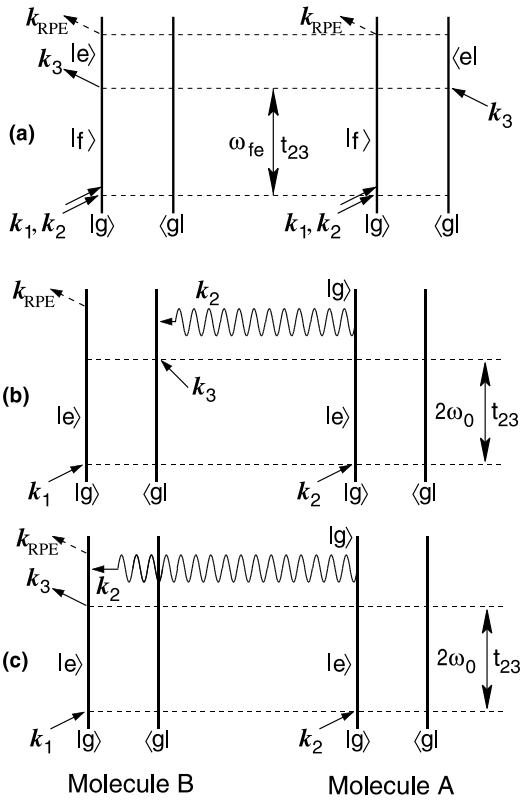

Fig. 1. (a) Double-sided Feynman diagrams representing the Liouville space pathways contributing to the third-order $\mathbf{k}_{\mathrm{RPE}} = \mathbf{k}_1 + \mathbf{k}_2 - \mathbf{k}_3$ signal in the rotating wave approximation induced by intermolecular coupling $t_{12} = 0$. During t_{23} the system is in a double quantum coherence $|f\rangle\langle g|$. (b) and (c) Feynman diagrams for the nonlinear response at $\mathbf{k}_{\mathrm{RPE}}$ induced by the local-field. Two different molecules are involved: The $\mathbf{k}_2$ field interacts with Molecule A, creating a delayed $\mathbf{k}_2$ local-field which subsequently interacts with Molecule B after $\mathbf{k}_3$. The original time ordering is destroyed, making the $\mathbf{k}_{\mathrm{RPE}}$ signal possible.

herence and the many-body density matrix undergoes a $2\omega_0$ oscillation. (ω_0 is a molecular transition frequency.) At no point during the process was a correlation created between largely separated molecules and the many-body density matrix is factorized into products of single molecule density matrices at all times.

To illustrate the differences between LF- and CI-resonances we present calculations for the RPE signal where we expanded the local-field to first order in ρ_0. We assume a model consisting of three two-level systems with different self-energies ϵ_1, $\epsilon_2 = 1.007\epsilon_1$, $\epsilon_3 = 1.01\epsilon_1$ and identical transition dipole moments μ interacting with three identical short pulses ($E_1(t-\tau_1) = E_2(t-\tau_2) = E_3(t-\tau_3)$) where the delay between the first two pulses is set to zero. The coupling between the systems is taken to be $J_{12} = J_{13} = J_{23} = -0.002\epsilon_1$ and in order to highlight the effects we used a small dephasing rate $\Gamma = 0.025J$ and set $(4\pi/3)\rho_0|\mu|^2$ which determines the relative strength of the LF-effects to be 0.2Γ. The two-dimensional spectrum is obtained from a Fourier transform of the heterodyne detected signal (Eq. (3)) with respect to the remaining delay t_1 between pulses 1, 2 and 3 and the delay t_2 between pulse 3 and the detection (see Eq. 31 of [16]). The conjugate frequencies are denoted Ω_1, Ω_2, respectively, and it is possible to retrieve the amplitude and the phase of the the signal, which are both discussed below (Figs. 2 and 3).

To discuss the resonances we introduce the following notation for the various possible states of this model: The states of the isolated two-level systems are $|i\rangle$ with energies ϵ_i and $|ij\rangle$ (with $\epsilon_{ij} = \epsilon_i + \epsilon_j$) denotes their combinations. Including coupling among the chromophores we obtain the single-exciton states $|\bar{i}\rangle(\epsilon_{\bar{i}})$ and two-exciton states $|\overline{ij}\rangle(\epsilon_{\overline{ij}})$ from diagonalization of the Hamiltonian. (Since we assumed a weak coupling the two-exciton states, which are linear combination of the product states $|\widetilde{ij}\rangle$ can be labeled according to their dominant contribution.) $|\widetilde{ij}\rangle(\epsilon_{\widetilde{ij}} = \epsilon_{\bar{i}} + \epsilon_{\bar{j}})$ denotes direct combinations of single-exciton states.

Fig. 2a shows the absolute value of the two-dimensional spectrum of independent systems; the entire signal is caused by local-field effects and on the Ω_1 axis we find peaks at direct combinations of the chromophore energies. For each $\Omega_1 = \epsilon_{ij}$ there are resonances at $\Omega_2 = \epsilon_i$ and $\Omega_2 = \epsilon_j$ where peaks at $(\Omega_1, \Omega_2) = (\epsilon_{ii}, \epsilon_i)$ are dominant. Overall there are nine peaks at six different Ω_1 values. The peaks in this local-field-induced signal only occur at combinations of single chromophore resonances and thus carry no new information. This in contrast to the CIMQC signal of coupled systems

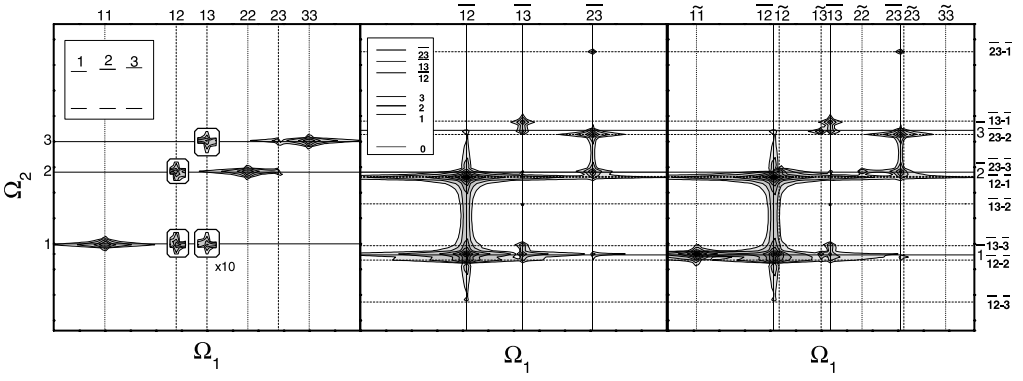

Fig. 2. Amplitude of the reverse photon echo signal of (a) three independent two-level systems without coupling (smaller peaks are zoomed by a factor of 10); (b) CIMQC signal and (c) the total signal for coupled systems. Solid vertical lines indicate energies of two-exciton states $|\overline{ij}\rangle$, dotted lines indicate twice the single-exciton ($|\widetilde{ii}\rangle$) (in (a) chromophore ($|ii\rangle$)) state energies and dashed lines indicate combinations of different single-exciton energies ($|\widetilde{ij}\rangle$). Similarly solid horizontal lines indicate single-exciton states ($|\bar{i}\rangle$), and dashed lines the energy differences between two- and single-exciton states. The contour lines are plotted at 1%, 2%, 5%, 10%, 20%, 40%, 60%, and 80% of the maximum of the RPE signal of coupled systems. The insets show the level scheme of the uncoupled (a) and coupled (b) systems.

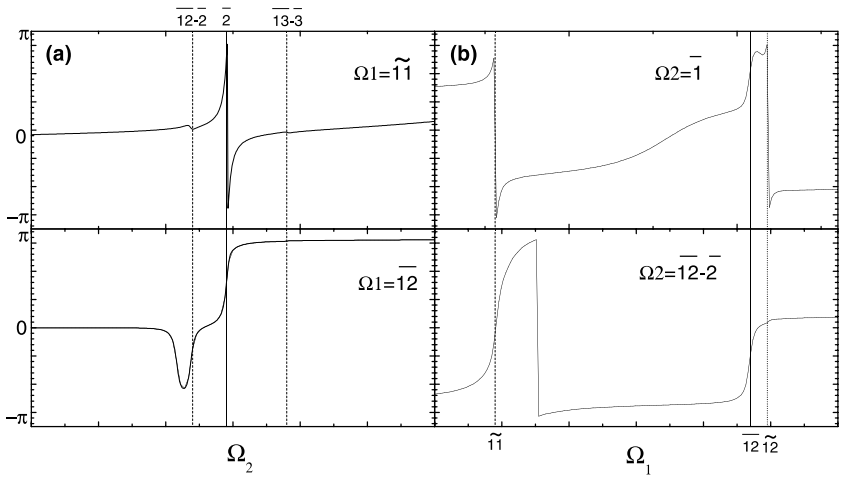

Fig. 3. Phase of the reverse photon echo signal of three coupled two-level systems at (a) two fixed values of Ω_1 and (b) two fixed values of Ω_2. In (a) the vertical lines indicate single-exciton states (solid) and energy differences between single- and two-exciton states (dashed) and in (b) the two-exciton state (solid) and product states of single excitons: **11** (dashed) and **12** (dotted).

where local-fields are neglected, is shown in Fig. 2b. Along the Ω_1 axis all peaks are located at two-exciton energies $\epsilon_{\overline{ij}}$. There are six possible peaks along the Ω_2 axis for each two-exciton state $\epsilon_{\overline{ij}}$: at all three possible single-exciton energies and at energy differences between the two-exciton state and the three-single-exciton states [22]. We thus get a maximum of 18 peaks. Fig. 2c displays the total signal including local-field and coupling effects. Along Ω_1 we find new resonances at combinations of single-exciton energies $\epsilon_{\widetilde{ij}}$, where in the case of CIMQC no peaks showed up. The new peaks have similar characteristics to Fig. 2a. Since most of the oscillator strength is in the lowest energy exciton ($J < 0$) the $(\epsilon_{\widetilde{11}}, \epsilon_{\overline{1}})$ peak is the most pronounced new feature, and, e.g. the resonance at $(\epsilon_{\widetilde{33}}, \epsilon_{\overline{3}})$ is too weak to be observed. Local-field resonances where Ω_2 corresponds to transitions from excited to two-exciton states could also be possible, but they are not seen because they are off-resonant and very weak.

Fig. 3 displays the phase of the total heterodyne detected signal as a function of Ω_2 (Fig. 3a) and Ω_1 (Fig. 3b) where the other frequency is held fixed. We can clearly see that the phase behaves qualitatively differently at LF- or CI-resonances. In Fig. 3a we display the phase of the signal for two different fixed values of Ω_1, where first the LF-peak at $(\epsilon_{\widetilde{11}}, \epsilon_{\overline{1}})$ and second the two peaks at $(\epsilon_{\overline{12}}, \epsilon_{\overline{12}} - \epsilon_{\overline{2}})$ and $(\epsilon_{\overline{12}}, \epsilon_{\overline{1}})$, which show mainly the CIMQC signal are probed. At $\Omega_2 = \epsilon_{\overline{1}}$ we find that while the LF-signal has a phase jump of 2π, the phase of the CIMQC-resonance changes by π. From Fig. 3b we also see qualitative differences in the phase as a function of Ω_1. The two displayed slices, at $\Omega_2 = \epsilon_{\overline{1}}$ and $\epsilon_{\overline{12}} - \epsilon_{\overline{1}}$, show strong differences at $\Omega_1 = \epsilon_{\widetilde{11}}$ (LF-resonance, dashed line) and at $\Omega_1 = \epsilon_{\overline{12}}$ (CI-resonance, solid line).

Since the local-field induced resonances arise from a reversal in time-ordering where the LF-signal is generated by the interaction with the free induction decay from another molecule after the last pulse acted (cf. Fig. 1b, c), the time-resolved LF-induced signal starts from zero and shows a rise since the probability for such an interaction increases linearly with time. On the other hand the CIMQC signal is directly generated by the interaction with the last pulse and subsequently should only show the dephasing decay. The combined dynamics of two molecules during t_1 should give oscillations with direct combinations of single-exciton frequencies and dephasing rates in the LF-signal vs t_1. While the high frequency was not yet experimentally resolved in optical RPE, the increased damping was observed in semiconductors [23]. The CIMQC signal should show oscillations

and dephasing corresponding to the two-exciton states. Figs. 2 and 3 show optical spectra; the corresponding NMR spectra will be different due to the reasons outlined earlier. However, the various types of resonances are identical and the figures illustrate the qualitative differences between them.

In the standard NMR treatment, short pulses can only create single quantum coherences since couplings among spins can be neglected during the pulses. However, the magnetic or optical response of a collection of two-level systems (spins or molecules) may show multi-quantum resonances, following two interactions with the fields. Our analysis reveals how high harmonic, multiparticle, resonances may be created by either local-field effects, or by direct intermolecular couplings. Both mechanisms require many particles. However, the former is a mean-field effective single-body effect: a field created by one molecule acts on a second one, whereas only the latter is a genuine many-body effect. Our calculations demonstrate that the LF-resonances carry no new microscopic information. In contrast, CIMQC reveal the details of intermolecular (or spin–spin) couplings and show specific fine structure shifts between ϵ_i, ϵ_{ij}, and $\epsilon_{\underset{\sim}{ij}}$ and different broadenings which depend on the local microscopic environments and dynamics. For LFMQC, the spins are not coupled and the total density matrix is factorized at all times into a direct product of single-particle matrices. Nevertheless, since the spins are driven by the same field, their motion is correlated thus creating a MQC. In order for this in-phase to be observable, it is crucial that the molecules communicate via the transverse local-field. Otherwise interference effects between various Liouville space pathways will exactly cancel these resonances in the nonlinear response since the system is harmonic and linear [12]. The resonances observed in multi-dimensional NMR in liquids are signatures of purely macroscopic local-fields and can be readily accounted for without alluding to long-range correlations among molecules separated by macroscopic distances. In contrast, for CIMQC, the spins are directly coupled and their state is correlated, i.e. the total density matrix may not be written as a direct product of the individual density matrices. In that case, the coupled system forms a multi-level system whereby multiple transitions are possible. Such CIMQC are created locally (e.g. between spins belonging to the same molecule).

A unified description of nonlinear optical spectroscopies of molecular aggregates described by the Frenkel–Heitler–London exciton Hamiltonian is provided by the nonlinear exciton equations (NEE) [13,25,22] which follow explicitly the time evolution of the multi-exciton variables $\langle B_m\rangle$, $\langle B_m B_n\rangle$, $\langle B_m^+ B_n\rangle$, and $\langle B_j^+ B_m B_n\rangle$. $B_n^+(B_n)$ is the creation (annihilation) operator for an excitation of the nth molecule. These constitute the complete set of dynamical variables required for the microscopic description of all spectroscopies which depend on the optical field up to third order. Higher variables including, e.g. four B_n factors only enter in higher order in the field. $\langle B_m B_n\rangle$ is responsible for two-exciton resonances, while $\langle B_m^+ B_n\rangle$ is the exciton density matrix responsible, e.g. for fluorescence and pump-probe spectroscopies. Closed expressions were derived for the third-order optical response by solving the NEE. The response is recast in terms of various exciton Green functions. This approach which describes the combined effects of exciton transport and two-exciton resonance sets the stage for designing multi-dimensional spectroscopies of excitons and analyzing them using coherence-transfer pathways. The NEE further provide a collective-oscillator picture for exciton dynamics and the optical response. Expressing the optical response through scattering of quasi-particles (rather than the more traditional picture of transitions among global eigenstates) provides an extremely useful physical insight at a greatly reduced computational cost.

Calculating CIMQC requires the explicit coupling and diagonalizing a many-body Hamiltonian. Computing LFMQC may be done in one of the two ways. We can stay at the single-particle level and replace the external driving field by a local-field, thus adding a nonlinearity to the problem [14]. The many-body aspects then enter only indirectly. Alternatively, one can consider explicitly many-body (two spin, three spin, etc.) variables such as $\langle B_n B_m\rangle$ even though they may be factorized as $\langle B_n\rangle\langle B_m\rangle$. Both descriptions are

equivalent but lead to a completely different physical picture. The choice is between having more variables vs extra nonlinearity. In contrast we do not have such freedom for the simulation of CIMQC, where a many-body formulation is essential.

In our analysis we have calculated the local-field to linear order in the incoming field. Other interesting optical many-body effects closely related to local-fields are known as *cascading* and come from nonlinear local-fields [12,20]. Cascading effects are very interesting and may contribute to the new resonances since as a result of cascading, E_1 may contain multiples of molecular frequencies ω_0. In our calculations we neglected cascading processes since local-field effects are enough to generate the new resonances. However they may yield interesting new effects in NMR. (e.g. higher harmonics $3\omega_0, 4\omega_0$, etc.)

Collective many-body effects have long been known in nonlinear optics of molecular aggregates and crystals in the frequency domain. These include the enhanced magnitudes of off resonant polarizabilities. In addition two quantum coherences lead to a structured two-photon manifold (ω_{gf} with various f states) which has been predicted [13,25] and observed [26] in pump-probe spectroscopy. Direct coupling is essential for these effects since the local-field mechanism gives a single two-photon resonance and grossly overestimates the magnitude of γ [13,15] which depends on a delicate balance of interfering contributions. Cooperative spontaneous emission (superradiance) observed in molecular aggregates is another signature of many-body effects [26]. Signatures of local-field and cascading have been also reported in femtosecond nonlinear spectroscopy [23,27–29]. The LFA resonances appear at frequencies $(\omega_{eg} + \omega_{e'g})$ and have dephasing rates $(\Gamma_{eg} + \Gamma_{e'g})$ which are sums of single-exciton values. In contrast, the corresponding CIMQC quantitaties ω_{fg}, Γ_{fg} are new values corresponding to the two exciton states. Experiments in GaAs semiconductor quantum wells showed local-field-induced $\mathbf{k}_{\mathrm{RPE}}$ (also denoted as photon echo with negative delay). They did not show two-quantum coherences but a dephasing rate $(2\Gamma_{eg})$ twice of that of the photon echo (where pulse 3 comes first) reflecting the excitation of two sites [23]. These resonances were simulated in molecular liquids [24]. Recently observed $\mathbf{k}_{\mathrm{RPE}}$ signals in gas-phase iodine originate from the local-field contributions discussed here [29]. Cascading effects were reported in femtosecond fifth-order Raman measurements in molecular liquids [30]. It will be interesting to explore the NMR analogues of these numerous many-body effects. Another prediction of the present work is that multiple high harmonic echoes ($2\omega_{eg}$ or ω_{fg}) should be directly observed in time domain $\mathbf{k}_{\mathrm{RPE}}$ four-wave mixing optical measurements involving high density of molecules and in semiconductors.

Acknowledgements

The support of The National Institutes of Health (GM59230-01A2) is gratefully acknowledged. We wish to thank Professors Jean Jeener, Jianhui Zhong and Warren Warren for their most helpful comments. The stay of A.T. in Rochester was funded by the Austrian Special Research Program F016 'ADLIS' (Austrian Science Foundation Vienna/Austria).

References

[1] G. Deville, M. Bernier, J.M. Delrieux, Phys. Rev. B. 19 (1979) 5666.
[2] J. Edzes, Magn. Reson. 96 (1990) 293.
[3] J. Bowtell, Magn. Reson. 100 (1992) 1.
[4] S. Lee, W. Richter, S. Vathyam, W.S. Warren, J. Chem. Phys. 105 (1996) 874.
[5] W.S. Warren, S.Y. Yang, S. Ahn, Y.Y. Lin, J. Chem. Phys. 116 (2002) 2075.
[6] J. Jeener, J. Chem. Phys. 112 (2000) 5091;
J. Jeener, Supplement of the Encyclopedia of Nuclear Magnetic Resonance, in press.
[7] J. Jeener, A. Vlassenbroek, P. Broekaert, J. Chem Phys. 103 (1995) 1309.
[8] M. Levitt, Concepts Mag. Reson. 8 (1996) 77.
[9] Y.-Y. Lin, S. Ahn, W.S. Warren, Science 290 (2000) 118.
[10] J. Baugh, A. Kleinhammes, D. Han, Q. Wang, Y. Wu, Science 294 (2001) 1505.
[11] W. Warren, Science 294 (2001) 1475.
[12] S. Mukamel, Principles of Nonlinear Optical Spectroscopy, Oxford University Press, New York, 1995.
[13] F.C. Spano, S. Mukamel, Phys. Rev. Lett. 66 (1991) 1197.
[14] S. Mukamel, Z. Deng, J. Grad, J. Opt. Soc. Am. B 5 (1988) 804.

[15] S. Mukamel, in: J. Zyss (Ed.), Molecular Nonlinear Optics, 1, Academic Press, New York, 1994.
[16] A. Tortschanoff, S. Mukamel, J. Chem. Phys. 116 (2002) 5002.
[17] C. Scheurer, S. Mukamel, Bull. Chem. Soc. Jpn. 75 (2002), in press.
[18] C. Scheurer, S. Mukamel, J. Chem. Phys. 115 (2001) 4989.
[19] H.A. Lorentz, The Theory of Electrons, Dover, New York, 1952.
[20] D. Bedeaux, N. Bloembergen, Physica 69 (1973) 67.
[21] D.P. Craig, T. Thirunamachandran, Molecular Quantum Electrodynamics, Academic Press, London, 1984.
[22] W.M. Zhang, V. Chernyak, S. Mukamel, J. Chem. Phys. 110 (1999) 5011.
[23] S. Schmitt-Rink, S. Mukamel, K. Leo, J. Shah, D.S. Chemla, Phys. Rev. A 44 (1991) 2124.
[24] J.A. Leegwater, S. Mukamel, J. Chem. Phys. 101 (1994) 7388.
[25] J. Knoester, S. Mukamel, Phys. Rev. A 39 (1989) 1899; Phys. Rev. A 41 (1990) 3812.
[26] H. Fidder, J. Knoester, D.A. Wiersma, J. Chem. Phys. 98 (1993) 6564;
S. DeBoer, D.A. Wiersma, Chem. Phys. Lett. 165 (1990) 45.
[27] J.C. Kirkwood, A.C. Albrecht, J. Raman Spectrosc. 31 (2000) 107.
[28] T. Efthimiopoulos, M.E. Movsessian, M. Katharkis, N. Merlemis, J. Appl. Phys. 80 (1996) 639.
[29] V.V. Lozovoy, I. Pastirk, M. Comstock, M. Dantus, Chem. Phys. 266 (2001) 205.
[30] D.A. Blank, L.J. Kaufman, G.R. Fleming, Chem. Phys. 111 (1999) 3105.